Steel and Composite Structures, *Vol. 30, No. 3 (2019) 217-230*
DOI: https://doi.org/10.12989/scs.2019.30.3.217

Experimental and numerical investigation of RC sandwich panels with helical springs under free air blast loads

Mohamed Rashad [1a], Mostafa M.A. Wahab [2] and T.Y. Yang [*3,1]

[1] *Department of Civil Engineering, University of British Columbia, Vancouver, Canada*
[2] *Department of Civil Engineering, Military Technical Collage, Cairo, Egypt*
[3] *International Joint Research Laboratory of Earthquake Engineering, Tongji University, Shanghai, China*

(*Received March 28, 2018, Revised December 10, 2018, Accepted January 25, 2019*)

Abstract. One of the most important design criteria in underground structure is to design lightweight protective layers to resist significant blast loads. Sandwich blast resistant panels are commonly used to protect underground structures. The front face of the sandwich panel is designed to resist the blast load and the core is designed to mitigate the blast energy from reaching the back panel. The design is to allow the sandwich panel to be repaired efficiently. Hence, the underground structure can be used under repeated blast loads. In this study, a novel sandwich panel, named **R**C panel - **H**elical springs- **R**C panel (RHR) sandwich panel, which consists of normal strength reinforced concrete (RC) panels at the front and the back and steel compression helical springs in the middle, is proposed. In this study, a detailed 3D nonlinear numerical analysis is proposed using the nonlinear finite element software, AUTODYN. The accuracy of the blast load and RHR Sandwich panel modelling are validated using available experimental results. The results show that the proposed finite element model can be used efficiently and effectively to simulate the nonlinear dynamic behaviour of the newly proposed RHR sandwich panels under different ranges of free air blast loads. Detailed parameter study is then conducted using the validated finite element model. The results show that the newly proposed RHR sandwich panel can be used as a reliable and effective lightweight protective layer for underground structures.

Keywords: lightweight sandwich panel; RHR; helical springs; free air blast loads; RHT

1. Introduction

Military underground structure is one of the most important infrastructures for military operations. These structures are expansive to build and requires robust protective layers to resist repeated blast loads. In the past, the entire protective layers are used as a sacrificial component, where it needs to be replaced after strong blast load (Vinson 2001, Zhu 2008, Nurick *et al*. 2009, Xia *et al*. 2016, Mazek and Mostafa 2013, Rashad 2013, Mazek 2014, Wahab and Mazek 2016). Sand layer is a common protective layer used for covering the underground structures. It has some disadvantages: (1) it is very heavy, which add significant loads to the underground structure. This makes the design of the underground structure uneconomical; (2) The sand layer cannot withstand repeated blast loads, after the first impact, the sand will be compacted and the entire underground structure will need to be rebuilt and; (3) It is very hard and expensive to control the sand density due to impaction and water drainage issues (TM5-1300 1990, UFC 3-340-02 2008).

To improve the performance of the military underground structure, lightweight blast protection layers are being developed. Lightweight blast protection layers offer many significant advantages: including (1) add minimum load to the existing structure; (2) can withstand repeated blast loads and; (3) can be replaced easily. One of such innovative lightweight protection layers is the **R**C panel - **H**elical springs- **R**C panel (RHR) sandwich panel. RHR sandwich panel consists of reinforced concrete panels and number of compression helical springs as an interlayer. RHR has a high strength to weight ratio and high energy dissipation capacity under large and repeated blast loads. RHR sandwich panel can be economically constructed and efficiently repaired after strong blast load without significantly affecting the design of underground structure.

The idea of RHR sandwich panel was first introduced by Rashad (2013), where detailed numerical study was conducted to examine the hyperdynamic response of the RHR sandwich panel. The concept of RHR was further used by Wahab and Mazek (2016), where experimental and numerical studies were presented. In these previous studies, the concrete panels were modeled using solid elements and the helical springs were modeled using a number of shell elements (shown in Fig. 1(a)). The result shows the approach of using shell elements for helical springs cannot accurately simulate the response of the helical springs. This is because the shell elements cannot accurately simulate the physical interaction between the coils during large blast loads. In addition, the use of the shell element will automatically assume the element has a virtual rectangular thickness which cannot accurately simulate the stress of the

*Corresponding author, Ph.D., P.Eng., Executive Director,
E-mail: yang@civil.ubc.ca
[a] Ph.D. Candidate,
E-mail: mohamed.rashad@alumni.ubc.ca

ISSN: 1229-9367 (Print), 1598-6233 (Online)

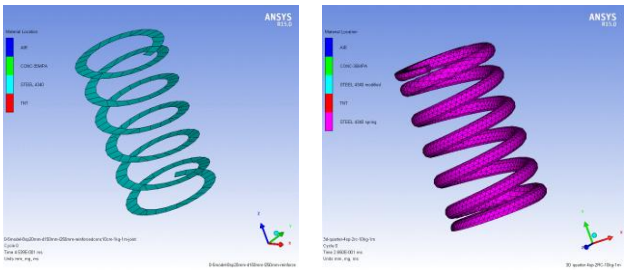

(a) Shell element (Rashad 2013 and Wahab and Mazek 2016) (b) 3D solid element (Current study)

Fig. 1 Helical spring modeling methods

circular wire. It is found that these factors have significant effects on the numerical behaviour of the proposed sandwich panel.

In this study, a modified solid element was proposed for the helical spring shown in Fig. 1(b). To effectively examine the performance of the RHR sandwich under free air blast loads, detailed numerical studies are conducted. The results are verified using available experimental test data conducted by the fortification team in the Egyptian army. The results show that the proposed numerical model can accurately model the hyperdynamic response of the RHR sandwich panel under free air blast load. In addition, the simulation results show that the RHR panel can be used as an efficient protective layer against large and repeated cycles of explosion loads.

2. Experimental study

To properly model the nonlinear dynamic response of the RHR sandwich under free air blast loads, four full scaled experimental tests are conducted. The first test is conducted to quantify the air pressure generated from the TNT charge detonation. The second, the third and the fourth tests are conducted to study the performance of RHR sandwich panel using 16 helical springs, as an interlayer between the two RC panels, under 1, 5 and 10 kg of TNT at a standoff distance (SoD) of 1 m, respectively. Fig. 2 shows the RHR sandwich panel which will be studied in this paper. The pressure time histories at different locations, maximum displacement of the front RC panel and the damage levels of the front, the back RC panels and the helical springs are recorded.

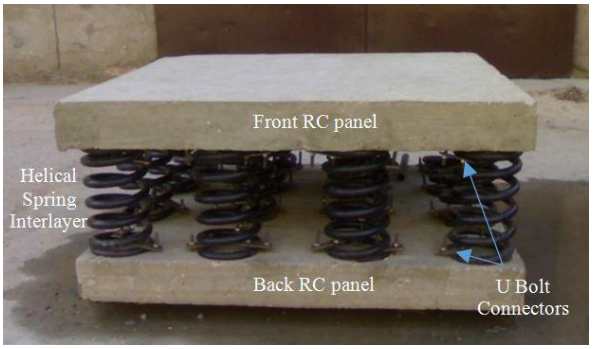

Fig. 2 RHR sandwich panel

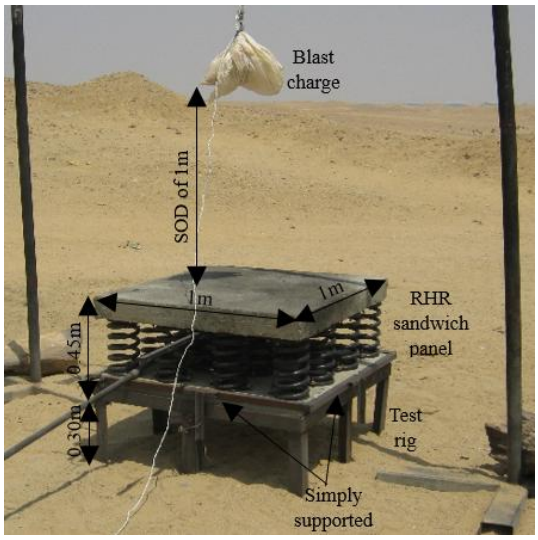

Fig. 3 Test rig

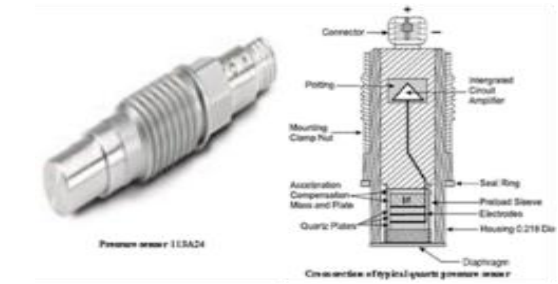

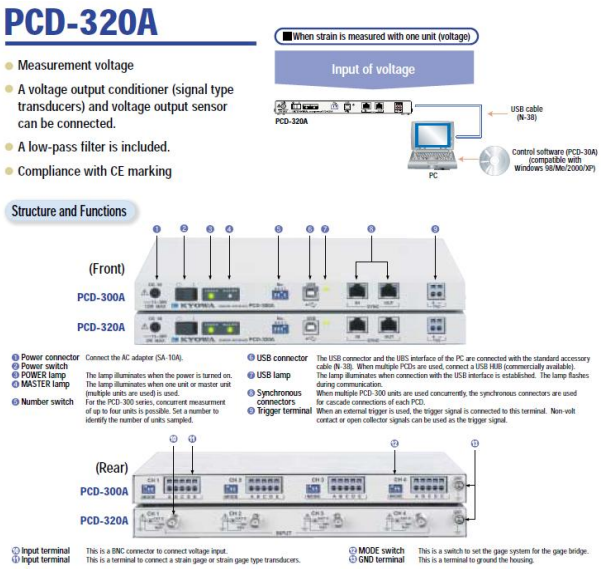

(a) Pressure sensor (b) PCD-320A transducer

Fig. 4 Voltage measuring instrument components

2.1 Test setup

The specimens are simply supported at the four edges of the back RC panel using the test rig, as shown in Fig. 3. The inner clear dimension of the test rig is 1 m × 1 m and it is raised 0.3 m from the ground to avoid the effect of the reflected shock wave on the specimen induced from the ground. The pressure-time histories are monitored using Piezotronics pressure smart sensor and PCD-320A transducer as shown in Figs. 4(a) and (b), respectively.

2.2 Specimen's preparation

Fig. 5(a) shows the helical springs used in this study. Sixteen compression helical springs are used in this arena tests. These helical springs are designed to withstand the applied blast load without reaching its closed length (fully compressed) and accordingly prevent the spring from reaching the plastic deformation level. Table 1 shows the specification of the helical springs.

The inner clear dimensions of the front and back RC panel formworks are 1 m × 1 m with thickness of 0.1 m. Each panel was reinforced with minimum flexural reinforcement with a single layer of 5Ø8 per meter. Fig. 5(b) shows the reinforcement layout. This minimum reinforcement prevents excessive cracking and deflection under self-weight. This reinforcement also prevents brittle failure under blast loads (TM5-1300 1990). U-bolts are added in the formworks to connect the helical springs to the RC panels. These connectors allowed the helical springs to be clamped with the two RC panels. The average compressive strength of concrete after 28 days was measured as 34.7 MPa.

Table 1 Specifications of helical springs used in the blast field test

Type of spring	Compression helical spring
Loose spring length	250 mm
Wire diameter	20 mm
Pitch of spring	46.3 mm
Outside spring diameter	150 mm
Mean Spring Diameter	130 mm
Inside Spring Diameter	110 mm
Spring Index	6.5 ul (unitless)
Spring weight	6.67 Kg

(a) Helical springs

(b) RC formwork

(c) RC panels

Fig. 5 Helical springs and RC formwork

3. Experimental test results

3.1 Free air blast load

To model the pressure generated by the free air blast load, a 1 Kg TNT is detonated at a SoD of 1 m. The pressure time history recorded in the field is compared with that calculated from the CONWEP program (CONWEP 1991) and that obtained from AUTODYN program (AUTODYN 2005). Figs. 6(a) and (b) show the test setup and a comparison of the pressure time histories obtained from AUTODYN, calculated from CONWEP and that recorded in the field, respectively. The results show less than 3% error between the simulated, the calculated and the measured pressure time histories.

3.2 1 Kg of TNT at SoD of 1 m

After verifying the free air blast load, the RHR sandwich panel is subjected to 1 Kg TNT detonated at a SoD of 1 m. Fig. 7 shows images of the specimen recorded

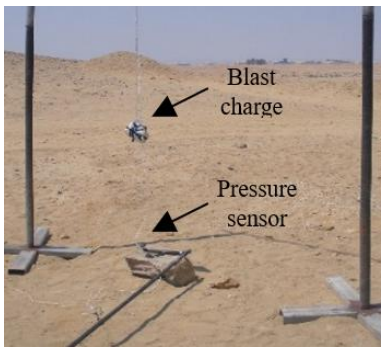

(a) Pressure sensor

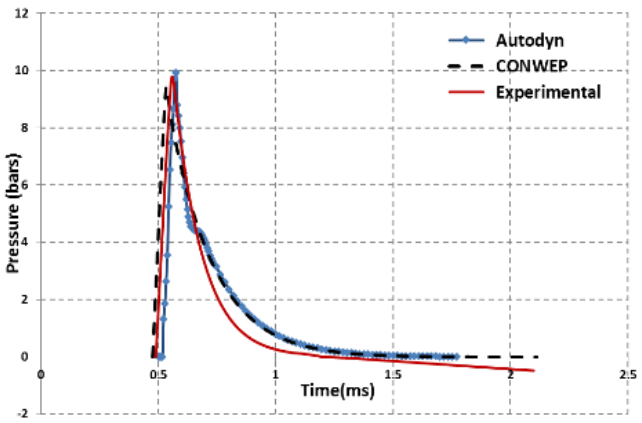

(b) Pressure-time histories

Fig. 6 Free air explosion test of 1 Kg TNT charge

by a high-speed camera, which can capture 20,000 frames/sec. The spreading of the fireball, the front shock wave (compressed air layer) and its reflection with the specimen surface and the ground surface are observed. Unfortunately, the deformation response of the specimen couldn't be captured by the high-speed camera as the specimen is covered with blast fireball after explosion. After the explosion process, it is observed that there are tiny hair cracks appeared on the front face of the front panel, as shown in Fig. 8(a). There was no visible damage occurs on the helical springs and the back panel.

3.3 5 Kg of TNT at SoD of 1 m

In this test, the tested RHR sandwich panel is subjected to 5 Kg TNT detonated at a SoD of 1 m. It is observed that significant cracks appeared on the front face of the front panel but the panel still in its coherent state. Based on the observation on the sides of the RC panel, some of the cracks penetrated through the front panel thickness. However, no visible damage occurs on the helical springs and the back panel. Fig. 8(b) shows some of the damage observed.

3.4 10 Kg of TNT at SoD of 1 m

In this test, the tested RHR sandwich panel is subjected to 10 Kg TNT detontaed at a SoD of 1 m. It is observed that the front panel is completely damaged and fractured into pieces. Those helical springs did fall off after the front panel fractured, but no visible damage on the helical springs is observed. There are a few hair cracks at the back face of the back RC panel. Fig. 8(c) shows some of the damage observed.

4. Verification and validation of the FE model

4.1 Blast pressure modelling

To properly model the behaviour of the TNT explosion, a numerical analysis is developed using AUTODYN program. The air block is modelled using the Hydro (ideal gas) equation of state (EOS), which can be written in the form of Eq. (1). TNT is modelled using the Jone-Wilkins-Lee (JWL) model (ANSYS 2007), which can be expressed in the form of Eq. (2). JWL model is used to simulate the rapid expansion of TNT explosion. After the TNT is detonated, the pressure created by the TNT detonation is modelled using ideal gas EOS. Table 2 shows the property of the air and the TNT used.

$$P_{EOS} = (\gamma - 1)\rho e \quad (1)$$

Where P_{EOS} is the pressure; γ is a constant; ρ is air density; e is the specific internal energy.

$$P_{EOS} = A\left(1 - \frac{w}{R_1 V}\right)e^{-R_1 V} + B\left(1 - \frac{w}{R_2 V}\right)e^{-R_2 V} + w\frac{E}{V} \quad (2)$$

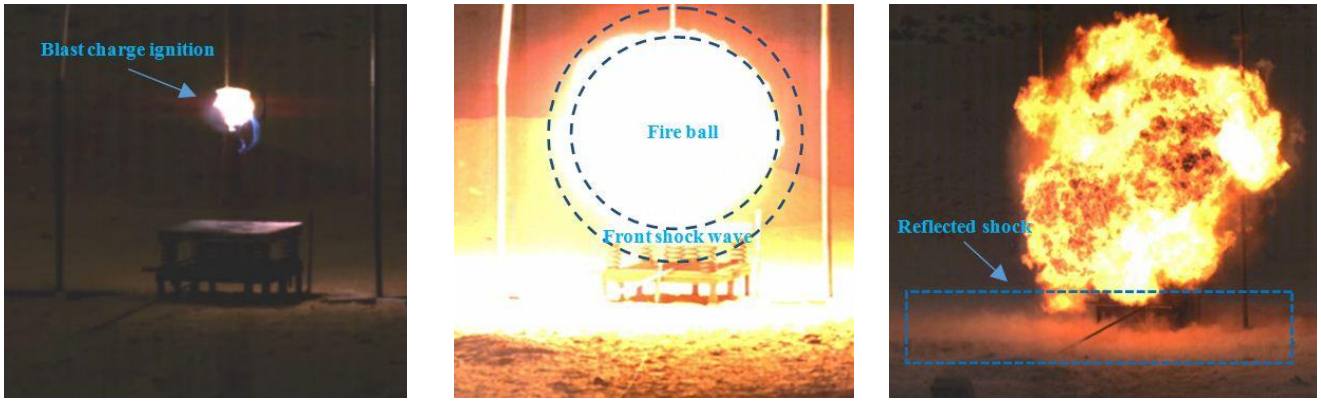

(a) 0.2 ms (b) 0.5 ms (c) 3 ms

Fig. 7 explosion process scenes of 1 kg TNT at SOF of 1 m

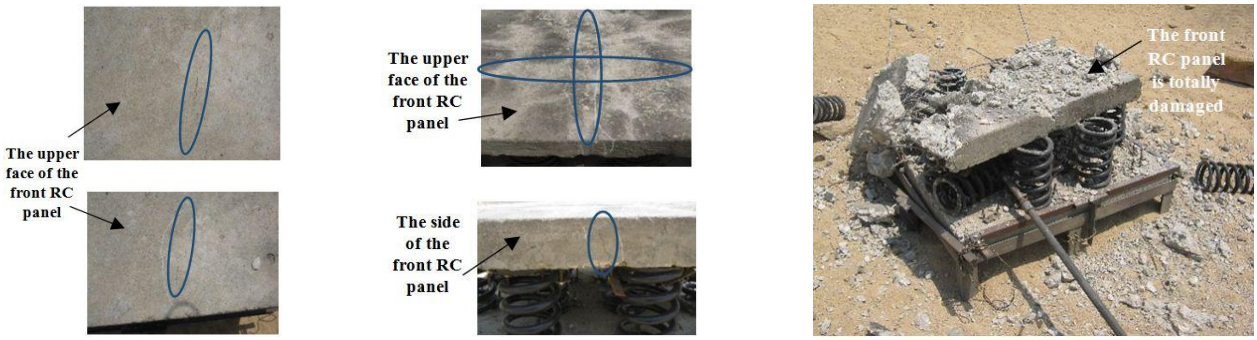

(a) 1 Kg TNT (b) 5 Kg TNT (c) 10 Kg TNT

Fig. 8 Damage observations of the RHR sandwich panel under different blast loads

Table 2 Material data of air and TNT used in the model

Material	Air	TNT	TNT (Ideal)
Equation of State	Ideal Gas	JWL	Ideal Gas
Initial Conduction	ρ = 1.225 × 10^{-3} g/cm^3	Default	From Detonation
Density	1.225 × 10^{-3} g/cm^3	Library Data	1.0 × 10^{-3} g/cm^3
Ideal Gas Constant	γ = 1.4	Standard	γ = 1.35
Reference Energy	2.068 × 10^5 µJ/mg		Model/remap data

Table 3 Summary of the parameters used to model TNT

JWL Parameter	TNT
A (GPa)	373.75
B (GPa)	3.747
R1	4.15
R2	0.90
w	0.35

where P_{EOS} is the hydrostatic pressure; A, B, R_1, R_2 and w are the JWL parameters which are used to model the air and TNT material; V is the ratio of ρ_{SOL}/ρ, where ρ is the current density and ρ_{SOL} is the density of solid explosive; $E = \rho_{SOL}\, e_{int}$ is the internal energy per unit volume of the explosive, where e_{int} is the current internal energy per unit mass; The specific values are outline in Table 3.

The pressure is firstly calculated in 2D model then mapped into 3D model, as shown in Fig. 9. This procedure is commonly used by explosive engineers to decrease the computational time needed to simulate the explosion process in a 3D finite element model (Rashad 2013, Rashad and Yang 2018). In the 3D model, Euler-FCT (Flux corrected Transport) formulation is used to solve the pressure time history. The boundary condition of the surrounding air is chosen as flow out at the six faces of the air block. Fig. 6(b) shows the pressure time history of a 1 Kg TNT detonated at a SoD of 1 m obtained from the numerical simulation, analytical analysis and experimental results. The results show good agreement between the trend of the three pressure-time histories.

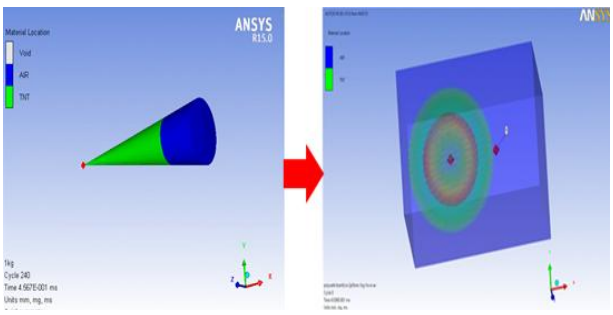

Fig. 9 Mapping from 2D to 3D model

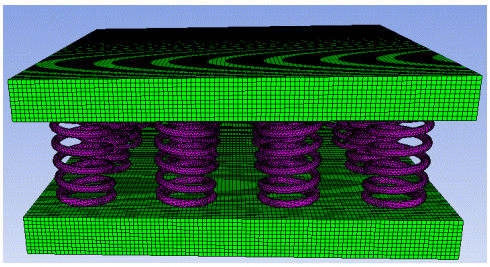

Fig. 10 A FE model of the RHR sandwich panel

4.2 Modelling of the RHR sandwich panel

The RHR sandwich panel, as shown in the Fig. 10, consists of two facing RC panels and sixteen helical springs, as an interlayer. In this section, modelling of each component of the RHR sandwich panel is validated individually before applying the numerical study on the entire sandwich panel.

4.2.1 RC panels modelling

In this study, concrete is modelled using both the porosity EOS and the polynomial solid EOS which can simulate the thermodynamic and the compaction behaviour of concrete at different levels of pressure (Herrmann 1969). **R**iedel-**H**iermaier-**T**homa (RHT) model (Riedel *et al*. 1999, 2008, Riedel 2000) is used as the concrete strength model. The RHT strength model employs three strength surfaces to define the elastic limit surface, failure surface and residual surface (or post-failure surface) as shown in Fig. 11. Tu and Lu (2009, 2010), Hu *et al*. (2016), Nyström and Gylltoft (2009, 2011), Wang *et al*. (2013) and Codina *et al*. (2016) showed the shortage of the default RHT model in simulating the accurate dynamic behaviour of concrete. Accordingly, a proposed modified RHT model is used to better simulate the concrete dynamic behaviour. Table 5 shows the mechanical properties of the concrete material which are used in this numerical study. Fig. 12 shows a comparison between the experimental and numerical observations of a plain concrete (PC) slab subjected to a blast load. More details can be found in ref. (Rashad and Yang 2019).

4.2.2 Helical spring and rebar modelling

There are different ways to model the helical spring, i.e., 2D beam elements with a virtual helical path (available in

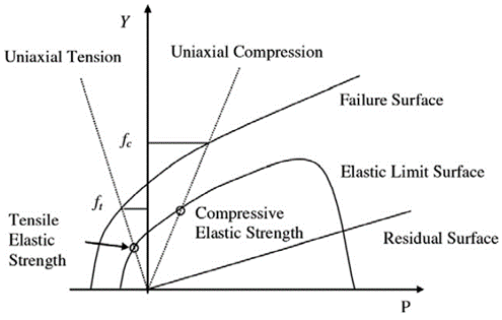

Fig. 11 Three strength surfaces of RHT model (Riedel *et al*. 1999)

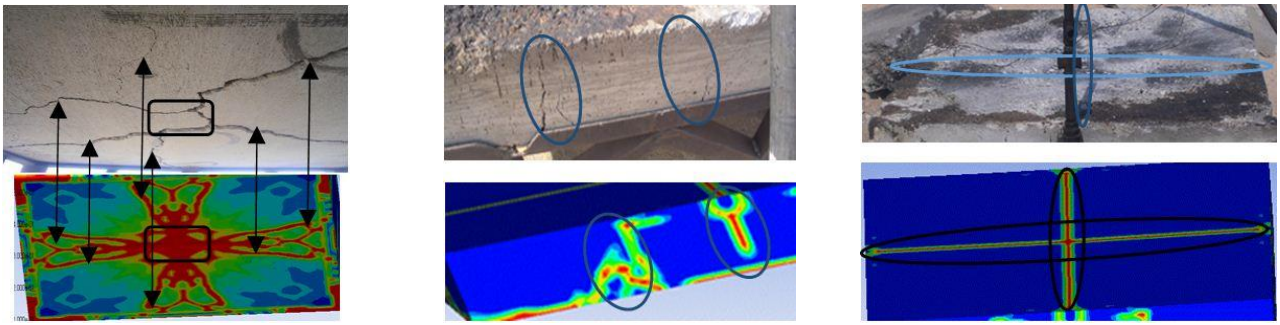

(a) Back Face (b) Side Face (c) Front Face

Fig. 12 Experimental and numerical damage observations on the plain concrete (PC) slab

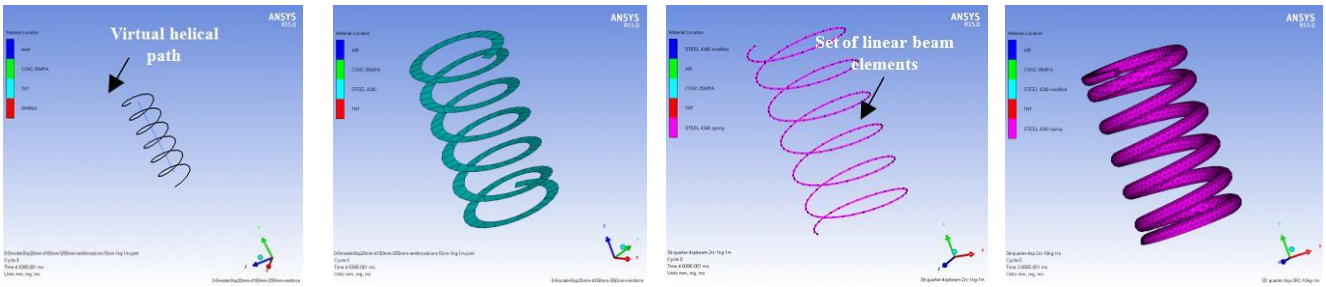

(a) AUTODYN beam elements (structured part) (b) Shell elements (unstructured part) (c) Beam elements (unstructured part) (c) 3D solid elements (unstructured part)

Fig. 13 kinds of helical spring simulation

Table 5 Material data of concrete material used in this study (AUTODYN 2005)

Equation of state	**P alpha**
Reference Density (g/cm^3)	2.75
Porous density (g/cm^3)	2.314
Porous soundspeed (m/s)	2.92 e+03
Initial compaction pressure (KPa)	2.33 e+04
Solid compaction pressure (KPa)	6.00 e+6
Compaction exponent	3
Solid EOS	Polynomial
Bulk modulus A1 (KPa)	3.527 e+7
Parameter A2 (KPa)	3.958 e+7
Parameter A3 (KPa)	9.04 e+6
Parameter B0	1.22
Parameter B1	1.22
Parameter T1 (KPa)	3.527 e+7
Parameter T2 (KPa)	0
Reference temperature (K)	300
Specific heat (J/kgK)	654
Thermal conductivity (J/mKs)	0
Compaction curve	Standard
Strength	**RHT concrete**
Shear modulus G (KPa)	1.67 e+07
Compressive strength f_c (KPa)	3.5 e+04
Tensile strength (f_t/f_c)	0.1
Shear Strength (f_s/f_c)	0.18
Intact failure surface constant A	1.6
Intact failure surface exponent N	0.61
Tens. /Comp. meridian ratio (Q)	0.6805
Brittle to ductile transition	0.0105
G (elastic)/(elastic-plastic)	2
Elastic strength f_t	0.7
Elastic strength f_c	0.53
Fractured Strength Constant B	0.9
Fractured Strength Exponent M	0.9
Compressive strain-rate exponent α	0.032
Tensile strain-rate exponent δ	0.036
Max. fracture strength ratio	1.00 e+20
Use CAP on elastic surface?	Yes
Failure	**RHT concrete**
Damage Constant D_1	0.02
Damage Constant D_2	1
Minimum Strain to Failure e_{min}^{fail}	0.002
Residual Shear Modulus Fraction	0.13
Tensile Failure	Hydro (P_{min})
Erosion	**Geometric strain**
Erosion strain	2
Type of geometric strain	Instantaneous

Autodyn), shell elements on a helical path, number of jointed beam elements on a helical path and 3D solid elements on a helical path. Fig. 13 shows some of the modeling approaches. After a detailed parametric study, it is found that the 3D solid element model gives more realistic behaviour than the beam element and shell element modelling, respectively. For using shell element, it is found that the spring behavior is less stiff than that in the physical test, the virtual cross section of the numerical spring wire is not circular as in reality. In addition, the spring continues to be compressed even after reaching its closed length. Accordingly, shell element gives inaccurate behaviour of the helical spring. The only disadvantage of the 3D solid element is the long computation time needed. 3D beam element can be used for obtaining a preliminary result limited to the displacement and the forces occurs in the axial direction of the beam element and ignoring the cross section and the lateral stress distribution on the wire (Shimozaki 1997 and Prawoto *et al*. 2008). In this study, helical springs are modelled using 3D solid element, as shown in Fig. 13(d), to study the accurate behaviour of the spring wire. The rebar is modelled by using beam elements. For the helical springs and the rebar, the steel elastic response range is modelled using Eq. (3). The steel plastic behaviour is modeled using the Johnson and Cook strength model (Johnson and Cook 1983) as presented in Eq. (4). Table 6 shows the properties of steel which are used for helical spring and rebar in this study, respectively.

Table 6 Material data of helical springs and rebar used in this study (AUTODYN 2005)

Equation of state	**Linear**	Strain rate constant (c)	0.014 / 0.022
Reference Density (g/cm^3)	7.83	Thermal softening exponent	1.03 / 1.00
Bulk modulus (kPa)	1.59 e+08	Melting temperature (k)	1.793 e+03 / 1.811 e+03
Reference temperature (k)	300	Ref. strain rate (/s)	1
Specific heat (J/kgK)	477.000092	Strain rate correction	1st Order
Thermal conductivity (J/mKs)	0	**Failure**	**Johnson Cook / None**
Strength	**Johnson Cook**	Damage constant D_1	0.05
Shear modulus (kPa)	8.18 e+07	Damage constant D_2	3.44
Yield stress (kPa)	7.92 e+05 / 3.5 e+05	Damage constant D_3	-2.12
Hardening constant (kPa)	5.10 e+05 / 2.75 e+05	Damage constant D_4	0.002
Hardening exponent	0.26 / 0.36	Damage constant D_5	0.61

$$P = K\,\mu \tag{3}$$

$$Y = \left[A + B\varepsilon_p^n\right]\left[1 + C\ ln\ \dot{\varepsilon}_p\right]\left[1 - T_H^w\right] \tag{4}$$

Where P is the pressure; K is the bulk modulus of the steel material; $\mu = (\rho/\rho_0 - 1)$ is the compression ratio; ρ_0 is the initial material density; Y is the yield strength; A is the yield stress at low strains; B is the strain hardening constant; ε_p is the effective plastic strain; n is the strain hardening exponent; C is the strain rate constant; $\dot{\varepsilon}_p$ is the normalized effective plastic strain rate; T_H is the homologous temperature given by $T_H = (T - T_{room})/(T_{melt} - T_{room})$; w is the thermal softening exponent.

5. Mesh sensitivity

Mesh size plays an important role in the accuracy and convergence of the finite element simulation. In this study, detailed mesh sensitivity study is conducted.

5.1 Air block

For the 2D explosion modelling, it is found that using element size of 1 mm is adequate to simulate the 1 Kg TNT denotation at SoD of 1 m, and 2 mm for the 5 Kg and 10 Kg TNT denotation at SoD of 1 m. The results give accurate maximum peak overpressures when compared with the calculated results from CONWEP software with accepted errors of 3.3%, 5.4%, and 5.9%, respectively. For the 3D explosion modelling, mesh sizes of 1, 2, 4, 6, 10, 15 and 20 mm are studied and evaluated. It is found that element size with thickness less than 10 mm usually creates too much computational time and memory allocation error (AUTODYN 2005). For element sizes of 10, 15 and 20 mm, the peak overpressure agrees well with that calculated from CONWEP with accepted errors of 3.9%, 6.1%, and 11.1%, respectively. Accordingly, the 10 mm mesh size is used for the 3D air block modelling. Using mesh size of 10 mm creates more than 2.5 million elements to simulate the blast load observed in the experimental test. Fig. 14 shows a comparison of the pear overpressure value calculated from the CONWEP and that simulated with the proposed mesh sizes in the 2D model and the 3D model.

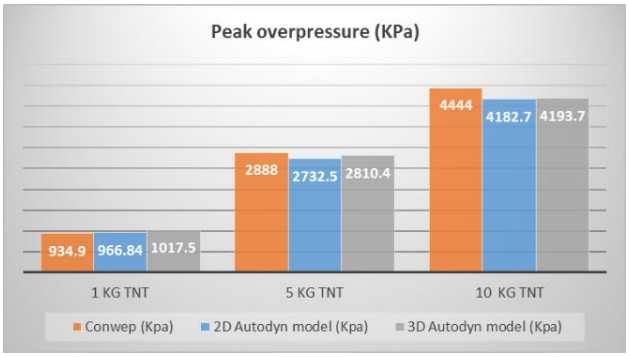

Fig. 14 Comparison of peak overpressure values

5.2 RC panels

An element size of 10 mm is adopted for the concrete panel to be consistent with the air block. It is found that the mesh size of 10 mm has enough accuracy for similar problems (Codina *et al*. 2016, Luccioni *et al*. 2013, Rashad 2013, Li *et al*. 2016). In addition, the element size of the donor boundary environment (applied load) should be equal or smaller than that of the acceptor body (RC slab) to obtain an accurate performance (AUTODYN 2005). This leads to use 25,000 elements to model the RC panel. A total of 24 elements are modelled for each rebar to ensure that each steel bar has sufficient number of elements and to be consistent with the RC panel nodes.

5.3 Helical springs

Two static analyses are conducted to calculate the spring stiffness and compare it with that measured by the compression test applied in the factory using the compression machine, as shown in Fig. 15(a). The first static analysis is performed using Inventor program (Autodesk Inventor 2017), as shown in Fig. 15(b). The result shows that the spring stiffness in the factory and that obtained from the static analysis agrees well with an acceptable error of 2.6%. The second static analysis is applied on the Ansys workbench, as shown in Fig. 15(c). Some trials are applied using different element sizes until reaching a good conformity between the physical stiffness and the numerical one with an acceptable error of 6.7%. Decreasing the element size more than the chosen value leads to increase the computational time. The number of elements used to model helical spring in this study is 16,645 solid elements. The result shows that such a mesh size can lead to accurately simulate the behaviour of the spring wire.

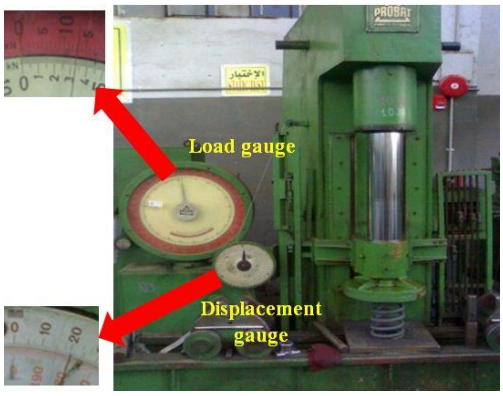

(a) Physical compression test (Rashad 2013)

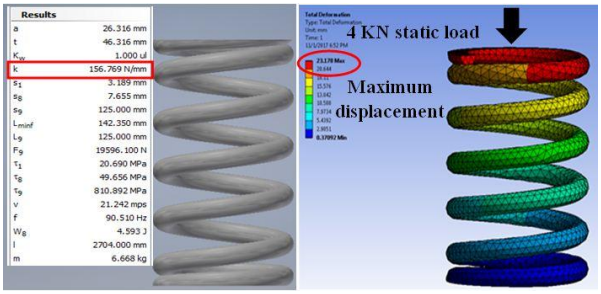

(b) Inventor program (c) Ansys workbench

Fig. 15 Helical spring stiffness measured in the factory and that obtained from the numerical static analyses

6. Numerical study of RHR sandwich panels

Due to double symmetry, a quarter numerical models are created. Consistent boundary conditions are applied to simulate a similar environment as in the arena test. Fully coupled Euler Lagrange interaction is adapted between the blast environment and the specimen. Trajectory interaction is adapted between the RC panels and the helical springs. This interaction is used for unstructured parts considering no external gap size between the Lagrange bodies even if the facing nodes of the adjacent bodies don't coincide. Fixed and movable gauges are created at different locations to record the pressure time histories, displacement time histories and internal energy time histories. In this study, the first peak of the displacement time history is studied. The damping effect has been neglected as it has no considerable effect on the first peak of the displacement time history (Hao *et al*. 1998, Wu *et al*. 1999). Fig. 16 shows the description and boundary conditions of a quarter model of the RHR sandwich panel.

In this study, the applied explosion energy has been dissipated by two main ways. First, the applied pressure is reflected by the front face of the front RC panel. Second, the front RC panel and helical springs absorb a portion of the applied energy. The function of the helical spring interlayer is absorbing a portion of the applied blast energy by applying a compression movement. Accordingly, extension forces are induced and act mostly upward which consequently extrudes the front RC panel to its original position after doing some oscillation. This wave diminishing is occurred due to the natural damping of the compression helical springs and its natural self-restoring (UFC 3-340-02 2008).

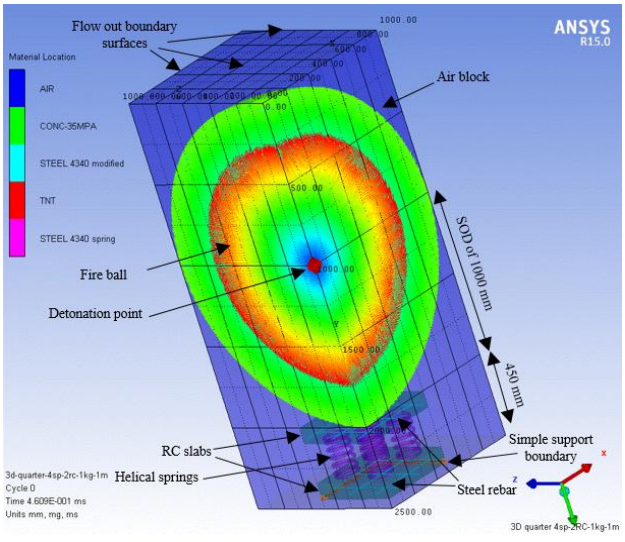

Fig. 16 A quarter model of RHR sandwich panel

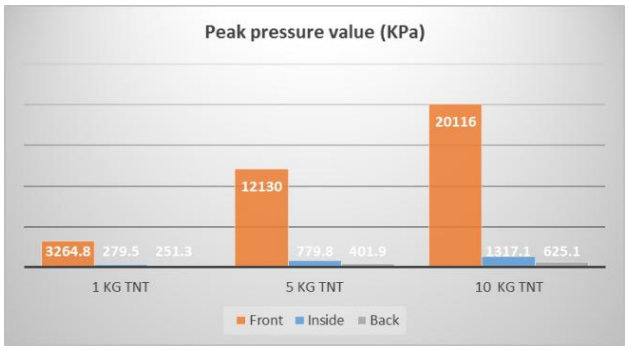

Fig. 17 Comparison of peak overpressure values at the front face of the front RC panel, midpoint of the RHR sandwich panel and back face of the back RC panel

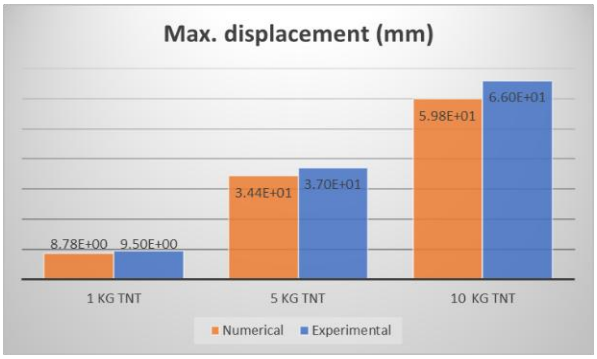

Fig. 18 Comparison between the maximum displacements of the front RC panel measured in the field and that obtained from the numerical analysis

7. Discussion of the results

Fig. 17 shows a comparison of the peak overpressure values at three different locations for three levels of blast loads. The results show that there are considerable reductions between the peak overpressure values at the front face of the front RC panel, midpoint of the RHR sandwich panel and back face of the back RC panel under the three different blast loads. The reduction percentages between the first and last values for 1, 5 and 10 Kg TNT detonated at SoD of 1 m are 92.3%, 96.7%, and 96.9%, respectively. These results indicate an excellent capability of the RHR sandwich panel of attenuating the effective pressure applied on the sandwich panel.

The main target of these studies is to protect the back RC panel (i.e., the main body of the underground structure) from being damaged. In order to achieve this goal, the displacement time histories and the damage level of the proposed sandwich panel components are analyzed. Fig. 18 shows a comparison between the maximum displacement of the front RC panel measured from the field tests and that obtained from the numerical analysis under the three different blast loads. The result shows excellent match between the experimental and the numerical simulations, where the errors are 7.7%, 8.5% and 9.2% for 1, 5 and 10 Kg TNT detonated at a SoD of 1 m, respectively. No considerable displacements are observed for the back panel in the three blast load cases.

The main target of these studies is to protect the back RC panel (i.e., the main body of the underground structure) from being damaged. In order to achieve this goal, the displacement time histories and the damage level of the

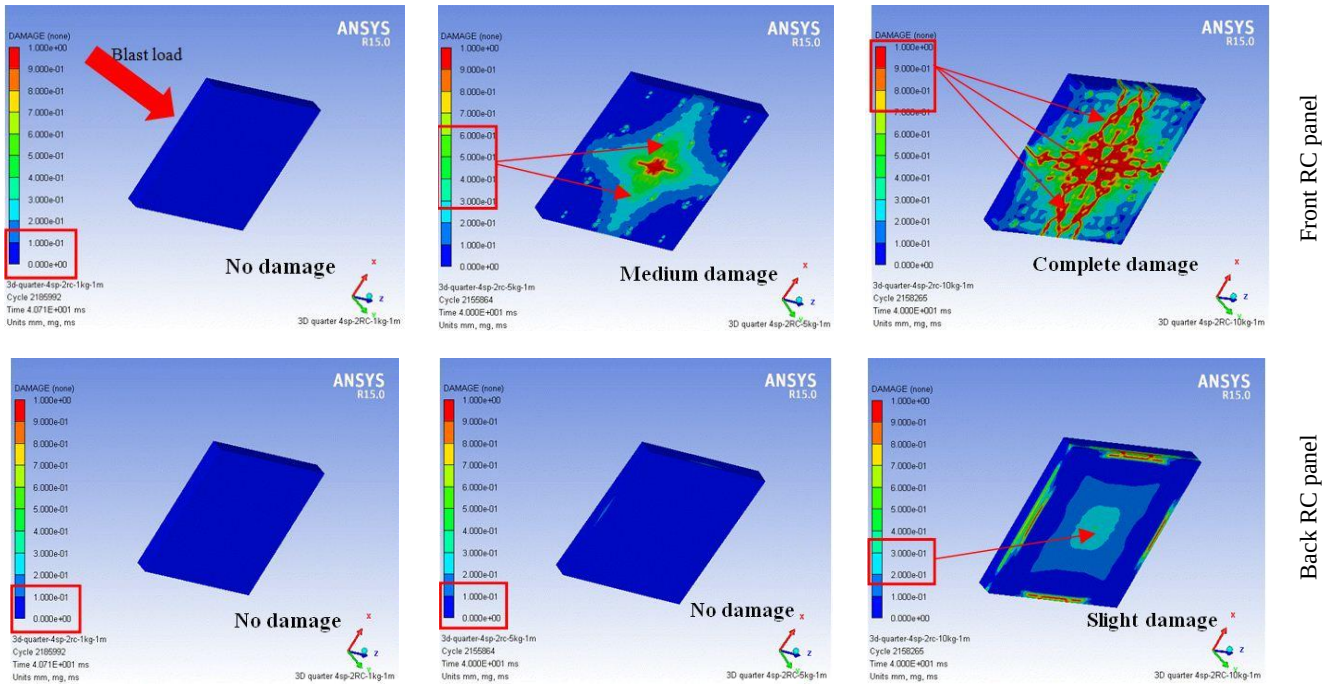

(a) 1 Kg TNT (b) 5 Kg TNT (c) 10 Kg TNT

Fig. 19 Damage contours of the front and back RC panels of the RHR sandwich panel subjected to 1, 5 and 10 Kg TNT

proposed sandwich panel components are analyzed. Fig. 18 shows a comparison between the maximum displacement of the front RC panel measured from the field tests and that obtained from the numerical analysis under the three different blast loads. The result shows excellent match between the experimental and the numerical simulations, where the errors are 7.7%, 8.5% and 9.2% for 1, 5 and 10 Kg TNT detonated at a SoD of 1 m, respectively. No considerable displacements are observed for the back panel in the three blast load cases.

For damage prediction analysis, Fig. 19 shows the damage contours of the front and back RC panels under the different blast loads. The damage level (DL) is a unit less measure for the damage and it can be categorized into four levels (Xu and Lu 2006, Zhou and Hao 2008, Wang and Zhang 2014): (1) no damage (DL = 0); (2) slight damage (DL = 0.1 to 0.3), where the panels experienced hair cracks; (3) medium damage (DL = 0.4 to 0.7), where the panel

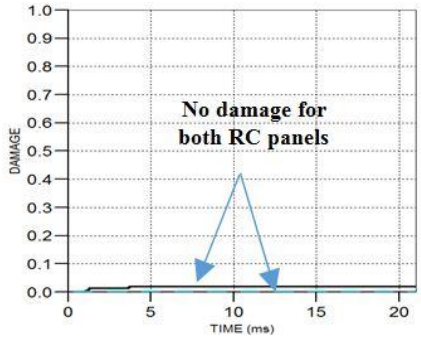

(a) 1 Kg TNT

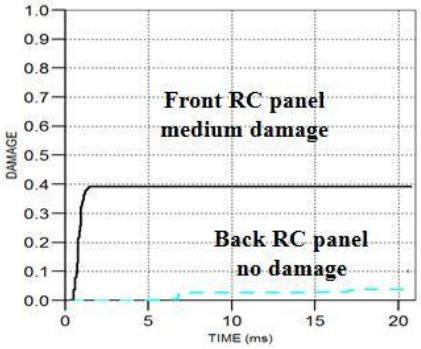

(b) 5 Kg TNT

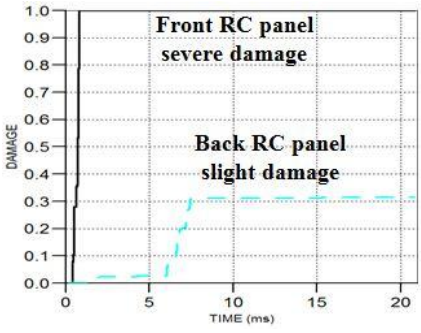

(c) 10 Kg TNT

Fig. 20 Damage level-time histories at the midpoints of the front and back RC panels of the RHR sandwich panel

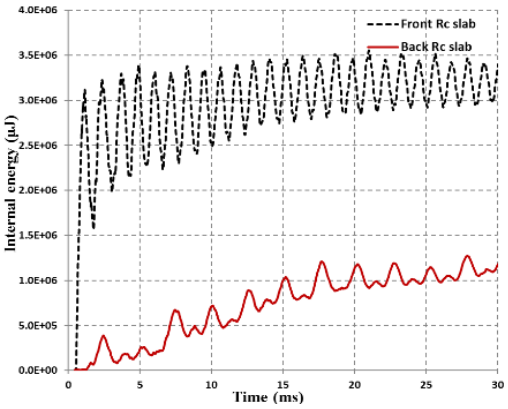

(a) 1 Kg TNT

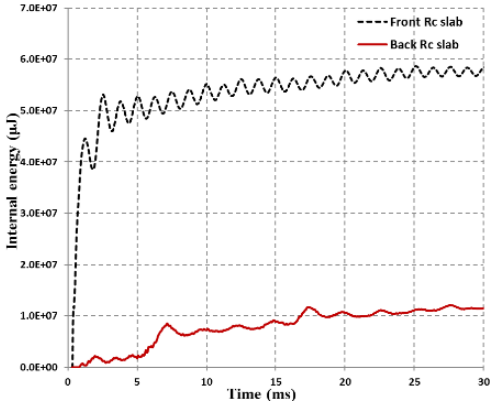

(b) 5 Kg TNT

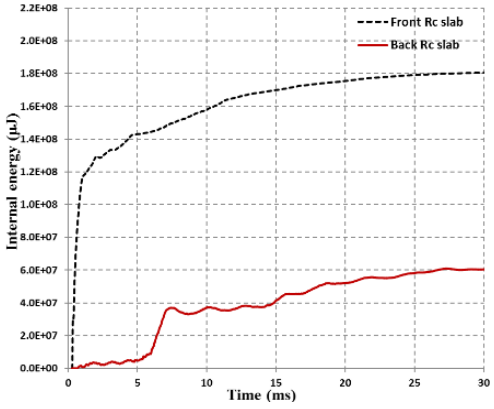

(c) 10 Kg TNT

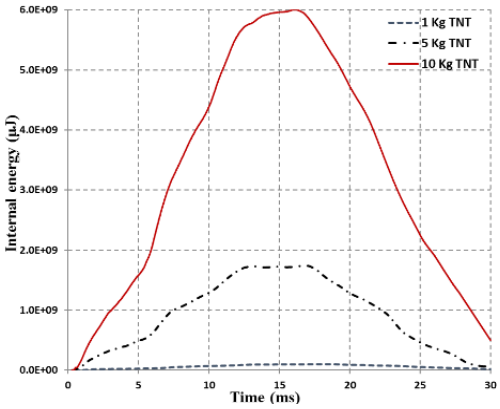

(d) Helical spring interlayer

Fig. 21 Internal energy-time histories of the front and back RC panel and helical spring interlayer

suffers significant cracks but still in the coherent state; (4) severe damage (DL = 0.8 to 1.0), where the panel is totally damaged and fragmented into pieces.

It is interesting to recognize that the front panel absorbed a considerable amount of applied blast energy. By increasing the blast load, damage level of the front panel increased significantly. Fig. 20 shows the DL time histories at the midpoint of the front and back RC panels under the three different loads. Accordingly, RHR sandwich panel can be used to withstand repetitive blast loads within the studied range without being damaged. For the case of 10 Kg TNT, the front RC panel needed to be replaced with a new one. Internal energy is one of the best evaluations for each component of the proposed sandwich panel. Internal energy time histories show that the amount of energy absorbed by each component of the sandwich panel separately. The goal of the proposed RHR sandwich panel is to minimize the total energy absorbed by the back panel (i.e., the main structure body). Fig. 21 shows the internal energy time histories experienced by the front RC panel, back RC panel and helical spring interlayer after explosion.

Fig. 21 shows that the front and the back RC panels tend to have a permanent plastic energy dissipation after having small elastic oscillation. The difference between the maximum plastic internal energy values absorbed by the front and the back RC panels under the three blast loads of 1, 5 and 10 Kg TNT are 62%, 80% and 80%, respectively. In contrast, the internal energy stored by the helical spring is released after experiencing the maximum displacement. The maximum internal energy stored the helical spring is approximately double the energy absorbed by the front RC panel. It is worth mentioning that the first layer is very effective in absorbing the applied energy. The remaining energy are stored in the helical springs then reflected. During this process some small amount of the applied energy is transmitted to the back panel. The result shows that the maximum value of the internal energy absorbed by the back RC panel is approximately 42% that of the front RC panel. The maximum displacement of the back RC panel, for the three different blast loads, is 0.082 mm which is negligible value. These results show the significant role of the helical spring interlayer in reducing the energy transmitted to the back RC panel. It should be noted that for the same blast load, by increasing the helical spring interlayer stiffness, the amount of applied energy transmitted to the back panel may be increased due to the rigidity of the helical springs which leads to early failure for both the front and the back RC panels. Hence, helical spring

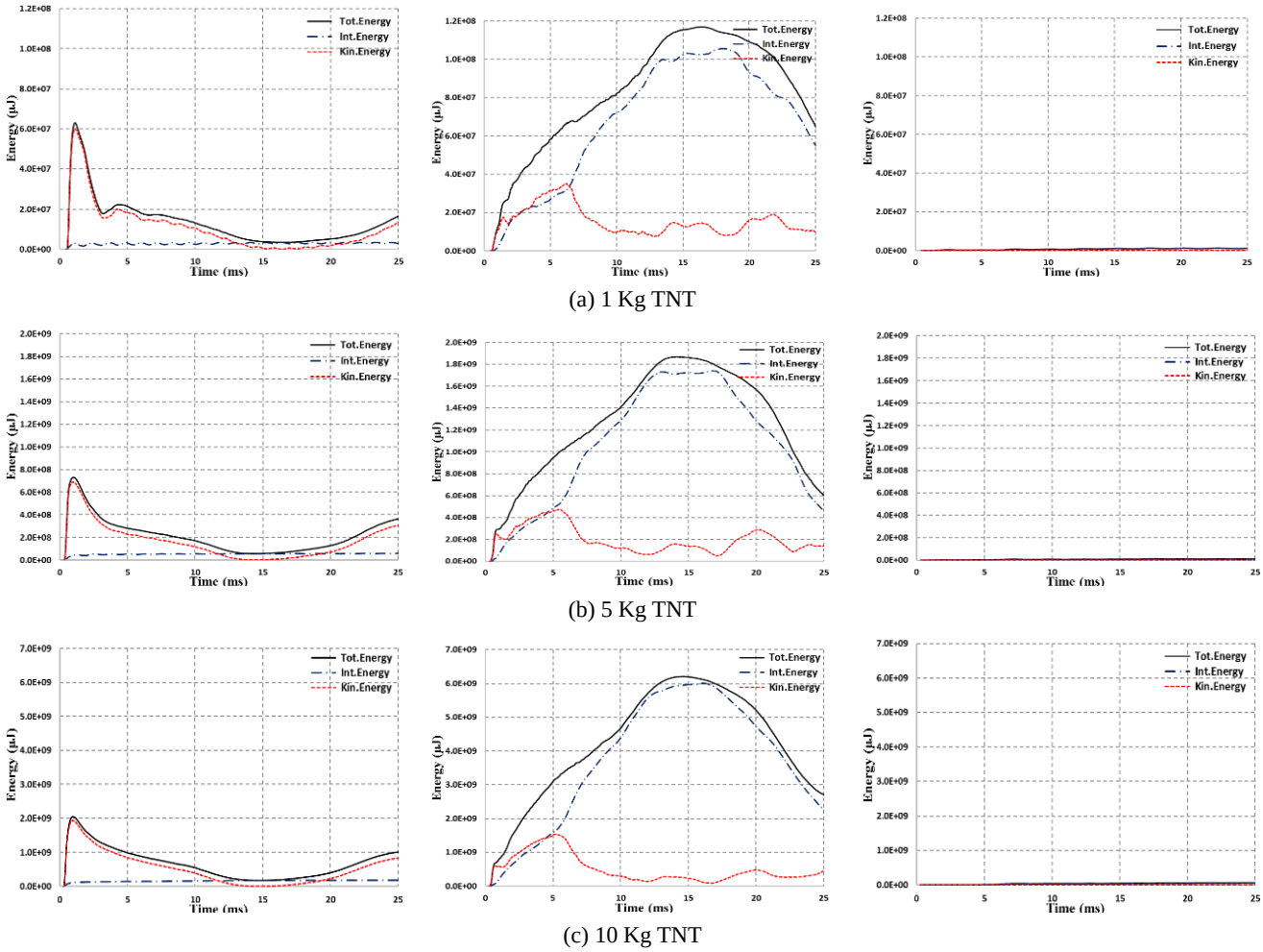

(a) 1 Kg TNT

(b) 5 Kg TNT

(c) 10 Kg TNT

Fig. 22 Total energy, internal energy and kinetic energy-time histories of front RC panel, helical spring interlayer and back RC panel in the cases of 1, 5 and 10 Kg TNT at SoD of 1 m, respectively

interlayer should be designed to be strong enough to absorb the shock wave without reaching its closed length and in addition, it should have the ability to reflect a considerable portion of the applied energy without damaging the back RC panel.

Fig. 22 shows the total energy, internal energy and kinetic energy time histories for the three main components of the RHR sandwich panel for the three blast loads. Total energy is the summation of the internal energy and the kinetic energy. It should be noted that due to the existence of the flexible supports (i.e., helical spring interlayer), the front RC panel dissipates a considerable amount of the applied blast energy in a form of kinetic energy as shown in Fig. 22(a). The kinetic energy applied in the front RC panel is higher than that applied in the helical springs, as shown in Figs. 22(a)-(b). In contrast, the internal energy stored by helical spring is higher than that of the front RC panels due to the resilience of the helical spring. As a result of a considerable amount of the applied energy dissipated by the front RC panel and the helical spring interlayer, the imparted energy to the back RC panel becomes small and it is mostly absorbed in a form of internal energy, based on the studied range of the blast load, as shown in Fig. 22(c). In general, the existence of helical spring interlayer has a considerable influence in enforcing the front RC panel to absorb its portion of the applied energy mostly in a form of kinetic energy and a small portion as internal energy. This performance leads to delay the full failure of the front RC panel and raise the value of the failure load. It should be mentioned that most of the applied energy is dissipated by the helical springs in a form of elastic internal energy in which it is completely released after the helical spring interlayer reaches its maximum displacement.

In addition, the plastic work done by the front and back RC panels under each blast load is analyzed. The results emphasize that the proposed system has a significant influence in attenuating the imparted energy reached the back RC panel. Fig. 23 shows a bar chart for the maximum plastic work done by each of the front and back RC panels. It is observed that the discrepancy between the maximum plastic work of the front and back RC panels, based on the three blast load cases of 1, 5 and 10 Kg TNT, are 92%, 94% and 69%, respectively. It should be noticed that on the case of 10 Kg TNT, the front RC panel damage allows

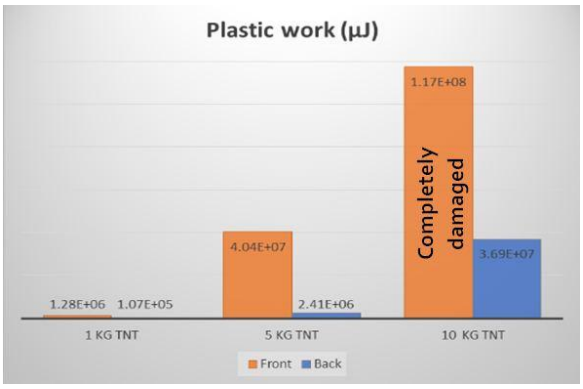

Fig. 23 Maximum plastic work done for the front and back RC panels of the RHR sandwich panel

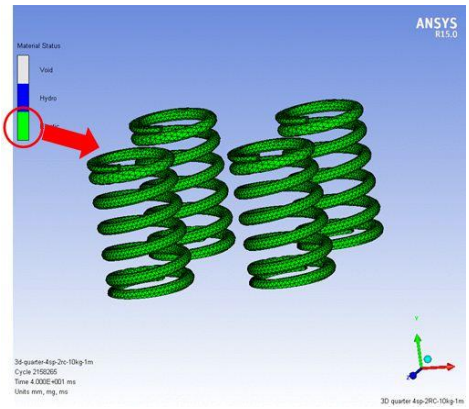

(a) Material status

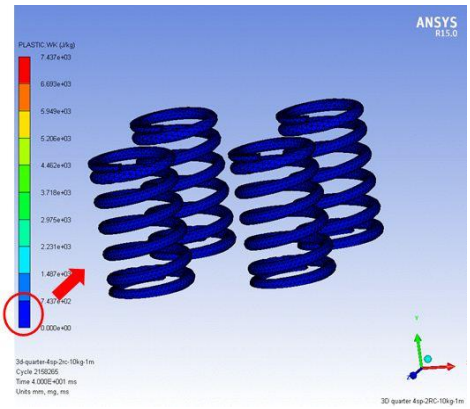

(b) Plastic work done

Fig. 24 The status of the helical spring under 10 kg TNT

a considerable amount of energy to be imparted to the back RC panel which leads to increasing the amount of the plastic work done by back RC panel. One of the main advantages of using the RHR sandwich panel is that the helical spring interlayer remains elastic. Hence, the RHR sandwich panel can be used to withstand another explosion, based on the studied range of blast loads up to 10 Kg TNT at standoff distance of 1 m. The material status of the helical springs and the plastic work done based on the 10 Kg TNT are shown in Figs. 24(a)-(b), respectively. The result shows the helical spring indeed remain elastic under the 10 Kg TNT detonated at SoD of 1 m.

8. Conclusions

Protective layers are one of the most important design components for military underground structures. The new trend of protective layer design focuses on using light weight material, which can be used for large and repeated blast loads and can be replaced and repaired efficiently.

In this study, a novel protective sandwich panel, named the RHR sandwich panel, is proposed. To properly examine the nonlinear dynamic behavior of the RHR panel, detailed experimental and numerical studies are conducted. The results show a conformity between the numerical and the corresponding experimental results. The following observations is obtained:

- For the free blast loading test, the difference between the simulated, calculated and measured pressure time histories is less than 3%.
- For the 2D explosion modelling, the difference between the numerical and calculated maximum peak overpressure for 1, 5 and 10 Kg TNT detonated at a SoD of 1 m are 3.3%, 5.4%, and 5.9%, respectively. For the 3D explosion modelling, errors are 3.9%, 6.1%, and 11.1%, respectively.
- To overcome the difficulty of simulating helical springs in AUTODYN, solid element model is imported in the AUTODYN program which revealed a more realistic behaviour than the other aforementioned modelling technics with an acceptable error of 6.7%.
- A good conformity between the experimental and the numerical behaviour of the RHR sandwich panel under different range of blast loads including the maximum displacement value of the RC panel and the damage level of the RC panels.
- An excellent matching between the experimental and the numerical maximum displacement values of the front RC panel, where the errors are 7.7%, 8.5% and 9.2% for 1, 5 and 10 Kg TNT detonated at a SoD of 1 m, respectively. No considerable displacements were observed for the back panel in the three blast load cases.
- The maximum value of the internal energy gained by the back RC panel is 42% that of the internal energy gained by the front RC panel.
- The reduction between the peak overpressure values at the front face of the front RC panel and back face of the back RC panel for 1, 5 and 10 Kg TNT detonated at SoD of 1 m are 92.3%, 96.7%, and 96.9%, respectively. There is an excellent capability of the RHR sandwich panel of attenuating the effective pressure applied on the sandwich panel.
- The discrepancy between the maximum plastic work of the front and back RC panels under the three load cases of 1, 5 and 10 Kg TNT detonated at SoD of 1 m are 92%, 94% and 69%, respectively.
- The proposed RHR sandwich panel is used as a protective layer to existing structures and also can withstand repetitive blast load without being damaged in the studied range. The only requirement is replacing the front RC panel in the case of 10 Kg TNT.
- The compression helical spring interlayer has a significant role in dissipating a considerable amount of the applied blast energy in a form of elastic energy. In addition, it helps in reducing the amount of energy absorbed by the front RC panel and that imparted to the back RC panel.
- Due to the existence of the helical spring interlayer, the reduction percentage between the internal energy absorbed by the front and back RC panels for the three blast loads 1, 5 and 10 Kg TNT are 62%, 80% and 80%, respectively.

Acknowledgments

The authors are grateful to the financial support by the Egyptian army, International Joint Research Laboratory of Earthquake Engineering (ILEE), National Science Foundation China (grant number: 51778486), Mitacs Globalink Research Award, the State Key Laboratory of Disaster Reduction in Civil Engineering in Tongji University and the State Key Laboratory of Disaster Prevention & Mitigation of the College of Defence Engineering of the Army Engineering University of PLA. Also, the authors are thankful to the manufactural assistance and the technical information provided by Military Technical College, Spring and Transport Needs Manufacturing Company, and Technical Research Centre in Egypt.

References

Ansys (2007), Theory reference manual; Release 11.0, ANSYS Inc., USA.

Autodesk Inventor (2017), Professional manual; Autodesk Inc., USA.

AUTODYN (2005), Theory manual revision 4.3; Horsham, Century Dynamics Ltd., UK.

Codina, R., Ambrosini, D. and Borbón, F. (2016), "Experimental and numerical study of a RC member under a close-in blast loading", *Struct. Eng.*, **127**, 145-158.

CONWEP (1991), Conventional Weapons Effects Program; US Army Waterways Experiment Station, Vicksburg, MS, USA.

Hao, H., Ma, G.W. and Zhou, Y.X. (1998), "Numerical simulation of underground explosions", *Fragblast Int. J. Blasting Fragment.*, **2**, 383-395.

Herrmann, W. (1969), "Constitutive equation for the dynamic compaction of ductile porous materials", *J. Appl. Phys.*, **40**(6), 2490-2499.

Hu, G., Wu, J. and Li, L. (2016), "Advanced Concrete Model in Hydrocode to Simulate Concrete Structures under Blast Loading", *Adv. Civil Eng.*, **2016**, 1-13.

Johnson, G.R. and Cook, W.H. (1983), "A constitutive model and data for metals subjected to large strains, high strain rates and high temperatures", *Proceedings of the 7th International Symposium on Ballistics*, The Hague, Netherlands, April.

Li, X., Miao, C., Wang, Q. and Geng, Z. (2016), "Antiknock performance of interlayered high-damping-rubber blast door under thermobaric shock wave", *Shock Vib.*, Article ID 2420893, 9 pages.

Luccioni, B., Araoz, G. and Labanda, N. (2013), "Defining erosion limit for concrete", *Int. J. Protect. Struct.*, **4**(3), 315-355.

Mazek, S.A. (2014), "Performance of sandwich structure strengthened by pyramid cover under blast effect", *Struct. Eng. Mech., Int. J.*, **50**(4), 471-486.

Mazek, S. and Mostafa, A. (2013), "Impact of a shock wave on a structure strengthened by rigid polyurethane foam", *J. Struct. Eng. Mech., Int. J.*, **48**(4), 569-585.

Nurick, G.N., Langdon, G.S., Chi, Y. and Jacob, N. (2009), "Behaviour of sandwich panels subjected to intense air blast - Part 1: Experiments", *Compos. Struct.*, **91**, 433-441.

Nyström, U. and Gylltoft, K. (2009), "Numerical studies of the combined effects of blast and fragment loading", *Int. J. Impact Eng.*, **36**(8), 995-1005.

Nyström, U. and Gylltoft, K. (2011), "Comparative numerical studies of projectile impacts on plain and steel-fiber reinforced concrete", *Int. J. Impact Eng.*, **38**(23), 95-105.

Prawoto, Y., Ikeda, M., Manville, S.K. and Nishikawa, A. (2008), "Design and failure modes of automotive suspension springs", *Eng. Fail. Anal.*, **15**, 1155-1174.

Rashad, M. (2013), "Study the Behavior of Composite Sandwich Structural Panels under Explosion Using Finite Element Method", M.Sc. Thesis; Military Technical College (MTC), Cairo, Egypt.

Rashad, M. and Yang, T.Y. (2018), "Numerical study of steel sandwich plates with RPF and VR cores materials under free air blast loads", *Steel Compos. Struct., Int. J.*, **27**(6), 717-725.

Rashad, M. and Yang, T.Y. (2019), "Improved nonlinear modelling approach of simply supported PC slab under free blast load using RHT model", *Comput. Concrete, Int. J.* [Accepted]

Riedel, W. (2000), "Beton unter dynamischen Lasten Meso- und makromechanische Modelle und ihre Parameter", Doctoral Thesis; Institut Kurzzeitdynamik, Ernst-Mach-Institut, der Bundeswehr Munchen, Freiburg, Germany. [In German]

Riedel, W., Thoma, K. and Hiermaier, S. (1999), "Penetration of reinforced concrete by BETA-B-500 numerical analysis using a new macroscopic concrete model for hydrocodes", *Proceedings of 9th International Symposium on Interaction of The Effect of Munitions with Structures*, Berlin-Strausberg, Germany, January.

Riedel, W., Wicklein, M. and Thoma, K. (2008), "Shock properties of conventional and high strength concrete, experimental and mesomechanical analysis", *Int. J. Impact Eng.*, **35**, 155-171.

Shimozaki, M. (1997), *FEM for springs*, Nikkan Kogyo Shimbunsha, Japan Society of Spring Engineers. [In Japanese]

Technical Manual TM5-1300 (1990), Structures to resist the effects of accidental explosions; U.S. Army, USA.

Tu, Z. and Lu, Y. (2009), "Evaluation of typical concrete material models used in hydrocodes for high dynamic response simulations", *Int. J. Impact Eng.*, **36**(1), 132-146.

Tu, Z. and Lu, Y. (2010), "Modifications of RHT material model for improved numerical simulation of dynamic response of concrete", *Int. J. Impact Eng.*, **37**(10), 1072-1082.

UFC 3-340-02 (UNIFIED FACILITIES CRITERIA), (2008), Structures to resist the effects of accidental explosions; U.S. Army corps of engineers, USA.

Vinson, J.R. (2001), "Sandwich structures", *Appl. Mech. Rev.*, **54**(3), 201-214.

Wahab, M.M.A. and Mazek, S.A. (2016), "Performance of double reinforced concrete panel against blast hazard", *Comput. Concrete, Int. J.*, **18**(6), 807-826.

Wang, G. and Zhang, S. (2014), "Damage prediction of concrete gravity dams subjected to underwater explosion shock loading", *Eng. Fail Anal.*, **39**, 72-91.

Wang, W., Zhang, D., Lu, F.Y., Wang, S.C. and Tang, F.J. (2013), "Experimental study and numerical simulation of the damage mode of a square reinforced concrete slab under close-in explosion", *Eng. Fail. Anal.*, **27**, 41-51.

Wu, C., Hao, H. and Zhou, Y.X. (1999), "Dynamic response analysis of rock mass with stochastic properties subjected to explosive loads", *Fragblast Int. J. Blast. Fragment.*, **3**, 137-153.

Xia, Z., Wang, X., Fan, H., Li, Y. and Jin, F. (2016), "Blast resistance of metallic tube-core sandwich panels", *Int. J. Impact Eng.*, **97**, 10-28.

Xu, K. and Lu, Y. (2006), "Numerical simulation study of spallation in reinforced concrete plates subjected to blast loading", *Comput. Struct.*, **84**(5), 431-439.

Zhou, X.Q. and Hao, H. (2008), "Numerical prediction of reinforced concrete exterior wall response to blast loading", *Adv. Struct. Eng.*, **11**(4), 355-367.

Zhu, F. (2008), "Impulsive Loading of Sandwich Panels with Cellular Cores", Ph.D. Dissertation; Swinburne University of Technology, Hawthorn, Australia.